ELSEVIER

Journal of Power Sources 70 (1998) 269–275

JOURNAL OF POWER SOURCES

Short Communication

Effect of curing on positive-plate behaviour in electric scooter lead/acid cells

Jenn-Shing Chen [a,*], L.F. Wang [b]

[a] *Department of Chemical Engineering, I-Shou University, Kaohsiung, Taiwan 84008, ROC*
[b] *School of Chemistry, Kaohsiung Medical College, Kaohsiung, Taiwan 80708, ROC*

Received 11 March 1997; accepted 27 March 1997

Abstract

This study investigates how curing temperature affects the composition and material structure of lead/acid positive plates. According to experimental results, the major morphology in positive active-material crystals is tribasic lead sulfate (= 3BS) at a low temperature and tetrabasic lead sulfate (= 4BS) at a high curing temperature (> 65 °C). Obviously, different curing conditions influence heavily electrode composition and cell performance. A driving pattern is developed for an electric scooter (ES) driving pattern according to urban driving pattern conditions (CNS-D3029). Three groups of cells with different curing temperatures (45, 65 and 85 °C) are subjected to two test methods: standard cycle testing, and ES-driving pattern cycle testing. The results demonstrate that the plates cured at the higher temperature contain less initial capacity but have a longer cycle life under both test conditions. © 1998 Elsevier Science S.A.

Keywords: Sealed lead/acid batteries; Lead/acid batteries; Electric scooters; Positive plates; Curing temperature

1. Introduction

Global environmental concerns have spurred efforts to develop electrically-powered vehicles. This alternative to conventional transportation is highly promising for a small Pacific island such as Taiwan, in which nearly 11.8 million motorcycles line the roads with an additional 0.8 million units being produced per month. This is equivalent to one motorcycle for every two the island's inhabitants. Unfortunately, this conventional mode of urban transportation has exacerbated island-wide the degeneration of air quality. To improve air quality, the Environmental Protection Administration (EPA) of the ROC has recently proposed mandating an annual sales quota of 2% of all motor cycles to be electric scooters (ESs) by the year 2000, i.e., a market potential of 20 000 ES annually. Correspondingly, governmental and other related agencies are expending considerable efforts to commercialize ES technology.

Two kinds of batteries are quite attractive/feasible for ES applications, namely, the valve-regulated lead/acid (VRLA) battery (Pb/PbO_2) and the nickel/metal-hydride battery (Ni/MH). Although the performance of Ni/MH is better than that of Pb/PbO_2, Ni/MH is economically unattractive for ES commercialization. For instance, the cost of the Ni/MH battery in the ES rivals the cost of the entire IC (internal combustion) motorcycle. Therefore, VRLA batteries will be used in commercial ESs.

The behaviour of the positive plates influences markedly the deep-discharge service of VRLA batteries. In the production of positive plates, the time, temperature and humidity during the curing process are critical in obtaining an active material with preferred chemical species and optimum morphology/porosity. Therefore, in this work, a study is made of the effects of curing temperature (45, 65 and 85 °C) on the composition and material structure of positive plates. Also, positive plates prepared with different curing temperatures are tested in sealed lead/acid cells under ES-driving patterns.

2. Experimental

2.1. Cell construction

Each cell contained two positive plates and three negative plates. The positive paste was prepared by mixing

* Corresponding author.

PII S0378-7753(97)02657-8

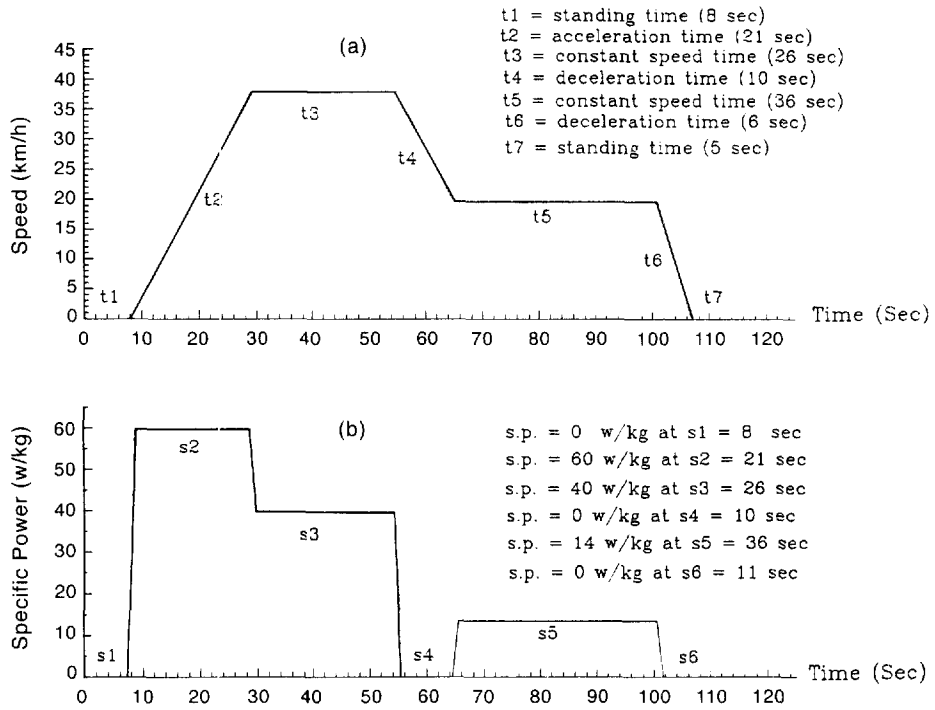

Fig. 1. (a) Velocity vs. time schedule for the CNS-D3029 test, and (b) the battery power required by the Improved Sanyang Dio Electric Scooter to negotiate the velocity schedule in (a).

leady oxide with water, sulfuric acid, and fiber. The paste composition was 50 kg ball-mill leady oxide, 6000 cm^3 water, 3500 cm^3 sulfuric acid (1.40 sp. gr.), and 50 g short fibres. Mixing was continued for 35 min and the apparent density of the paste was 4.1 g cm^{-3}. Next, the paste was applied to grids cast from a Pb–Ca alloy. The grid dimensions were: 69 mm × 40 mm × 3.6 mm. The positive plates were controlled with around 33 g paste on both sides of each grid and, then, were cured. Curing was performed for one day at temperatures of 45, 65 and 85 °C at a relative humidity of > 90%. Prior to formation, the plates were dried in air about 3–5 days until the moisture in the paste was < 1 wt.%. The current density was controlled at 6 mA cm^{-2} and the formation capacity had a theoretical capacity of about 200%. After formation, the plates were washed in running water for several hours and then dried in an oven at 65 °C for 24 h. All negative plates and absorptive glass-mat (AGM) separators used in the work were supplied by Ztong Yee Battery Corporation (Taiwan). Each cell was filled with 38 cm^3 of electrolyte and then sealed with a cover. In all experiments, the electrolyte was sulfuric acid solution with a sp. gr. of 1.335 (20 °C). The rated capacity of the cell was 4 Ah.

2.2. Cycling tests

The cells were cycled under computer-controlled charge and discharge regimens using Arbin Battery Testing Sys-

Table 1
Comparison of phase composition and BET specific surface area of paste, cured and formed active-material

Sample	Composition wt.% (±4%)								BET specific surface area ($m^2\ g^{-1}$)
	Pb	α-PbO	3BS[a]	4BS[b]	HC-PbO[c]	α-PbO_2	β-PbO_2	$PbSO_4$	
Paste	5.1	59.1	35.8						1.0395
45 °C curing									
After curing		56.6	39.9		3.5				0.8502
After formation						13.5	82.9	3.6	4.3213
65 °C curing									
After curing		29.8	9.5	59.1	1.6				0.5538
After formation						31.5	64.3	4.2	3.3556
85 °C curing									
After curing		37.6		62.4					0.3149
After formation						43.7	50.6	5.7	2.8002

[a] $3PbO \cdot PbSO_4 \cdot H_2O$.
[b] $4PbO \cdot PbSO_4$.
[c] $2PbCO_3 \cdot Pb(OH)_2$.

tems. To render the cell active, all cells were charged at 0.23 A for 13 h before regular cycle testing. Two test methods were employed: standard cycle testing and ES-driving pattern cycle testing. Standard cycle testing used a discharge current of 0.8 A to a 1.75 V cell cut-off voltage and a charge current of 0.4 A to 120% of the previous discharge capacity. In addition, an open-circuit period of 30 min was implemented at the end of each half-cycle. Cycling continued until the cell capacity dropped and remained below 80% of the initial capacity. The ES-driving pattern in Fig. 1(b) was derived from using of the *Chinese National Standard-D3029* (*CNS-D3029*) driving schedule (Fig. 1(a)) as negotiated by an Improved Sanyang Dio electric scooter [1]. In the *CNS-D3029*, the scooter must rest for 8 s, accelerate from zero to 38 km h^{-1} in 21 s, cruise at 38 km h^{-1} for 26 s, decelerate and brake to 20 km h^{-1} in 10 s, cruise at 20 km h^{-1} for 36 s, decelerate and brake to a stop in 6 s, and rest for 5 s. After 112 s, the schedule repeats itself. This average velocity is 22.5 kmh^{-1} and a scooter travels ~0.7 km during one cycle of the schedule. Thus, the ES-driving pattern cycle test takes 112 s, and has six steps and four power levels. In the ES-driving cycle testing, the cells were cycled under the following procedure: a constant power discharge according to each step power on the schedule was repeated until the cell voltage fell below 1.75 V/cell and a 0.4 A charge current to 120% of the previous discharge capacity. Finally, an open-circuit period of 30 min was implemented at the end of each half-cycle.

2.3. Analysis of positive-plate material

The physicochemical properties of the positive active-material, including the phase composition, morphology and specific area (porosity), were obtained by X-ray powder diffraction (XRD), scanning electron microscope (SEM), and BET-N_2 adsorption. All analytic samples taken from the plates were treated via the following steps [2]: (i) wash with distilled water (to remove acid); (ii) wash with absolute ethanol (to remove water) and dry in a desiccator; (iii) after drying, a portion of each sample was ground gently using a pestle and mortar.

3. Results and discussion

3.1. Analyses of plate composition and morphology

Table 1 presents the physicochemical and XRD analyses of all sulfate in the paste (before curing), in plates after curing at 45, 65, and 85 °C, and in plates after formation. The results show that the major paste constituent is α-PbO and tribasic lead sulfate (3BS) together with some lead. During paste mixing, the temperature is maintained below ~50 °C and tetra basic lead sulfate (4BS) is not found in the paste. 4BS is formed preferentially at a temperature exceeding ~70 °C [2–4]. The chemical composition of the cured plates relies heavily on the temperature conditions that are applied during the curing process. At 45 °C, the predominant species are 3BS and unreacted α-PbO. Increasing the curing temperature causes the 4BS to grow and the amount of 3BS to decrease. At 85 °C, only 4BS and α-PbO are found in the plate composition. Many formation studies [5–7] have shown that 4BS favours the formation of α-PbO_2, and that 3BS yields β-PbO_2. Indeed, the data in Table 1 reveal that the formation of 3BS-rich plates leads to a higher β-PbO_2 content than that in 4BS-rich plates. Moreover, the β-PbO_2 phase forms in proportion to the 3BS content.

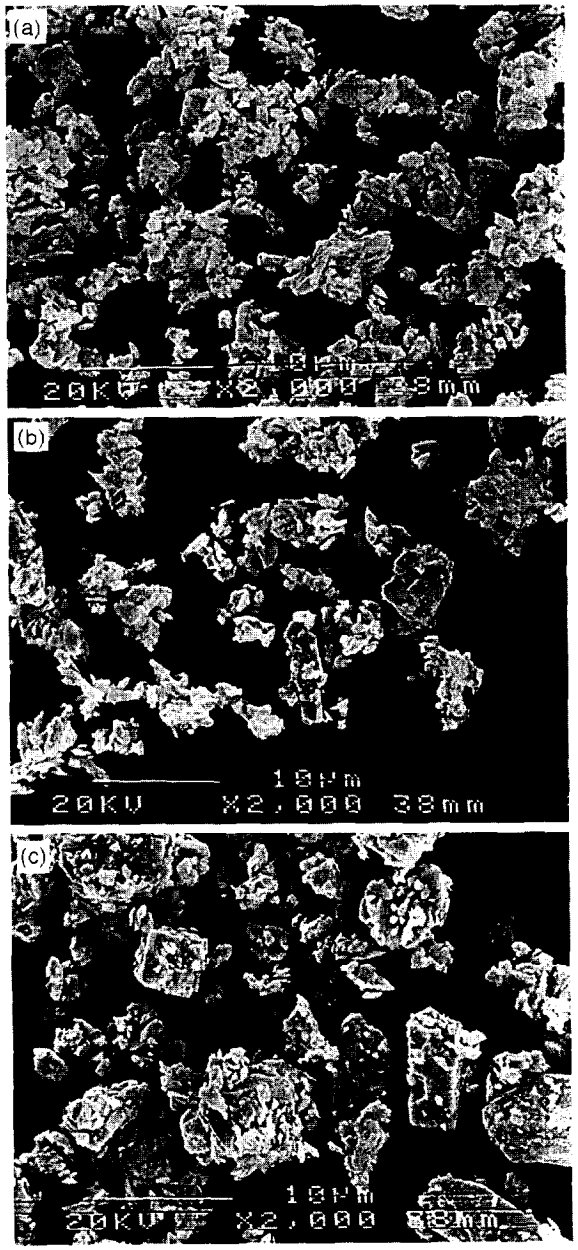

Fig. 2. Scanning electron micrographs of cured crystals at curing temperatures of: (a) 45 °C; (b) 65 °C; (c) 85°C.

Table 2
Cycle-life performance data for representative groups of 4.0 Ah VRLA cells

Sample	Cycle no.	Initial capacity (Ah)	Capacity loss/cycle (%)	Average capacity/cycle (Ah)
45 °C curing: Group A				
A1	140	4.15	0.159	3.87
A2	152	4.08	0.147	3.84
A3	150	4.09	0.149	3.80
A4	142	4.10	0.157	3.73
A5	134	4.16	0.166	3.83
65 °C curing: Group B				
B1	180	3.87	0.124	3.71
B2	175	3.92	0.127	3.81
B3	166	3.95	0.134	3.72
B4	183	3.89	0.122	3.67
B5	168	3.90	0.132	3.58
85 °C curing: Group C				
C1	193	3.78	0.116	3.77
C2	185	3.81	0.120	3.67
C3	180	3.82	0.124	3.70
C4	188	3.76	0.119	3.69
C5	178	3.75	0.125	3.53

The 4BS and α-PbO_2 crystals are larger than the respective 3BS and β-PbO_2 crystals. Hence, the pore surface area is small. Table 1 also indicates that the cured plates contain more 4BS crystals and have a smaller BET specific surface area. Formed plates with more α-PbO_2 exhibit a smaller BET specific surface area. Fig. 2 presents scanning electron micrographs of cured crystals at different curing temperatures. The cured paste consists of large crystals of 4BS or 3BS together with smaller crystals of PbO. Both types of 3BS and 4BS crystals have an elongated prismatic form, but 4BS crystals are considerably larger due to a higher crystal growth rate and a rather low nucleation rate [2,8,9]. The cured crystals formed at 85 °C (Fig. 2(c)) are clearly larger than those formed at a lower temperature (cf. Fig. 2(a) and (b)).

3.2. Cell standard cycle-life performance

This work also attempts/aims to determine the effects of three different curing temperatures (45, 65 and 85 °C) on cell performance. Three groups of cells with different curing temperatures were subjected to two test methods, namely, standard cycle testing and ES-driving pattern cycle testing. Five cells in each group were subjected to standard cycle-life testing to assess the influence of the three different curing temperatures. Table 2 lists the values

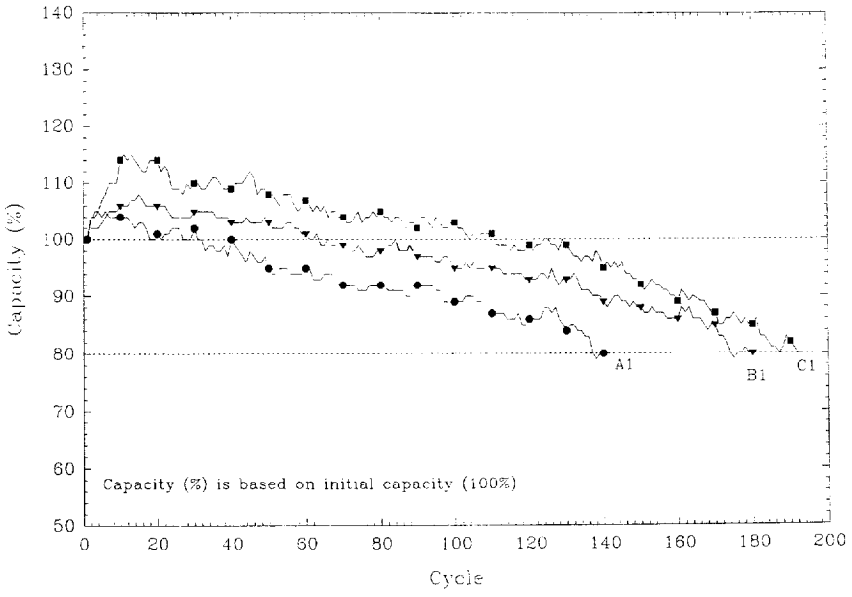

Fig. 3. Capacity vs. cycle number for the cells A1, B1 and C1.

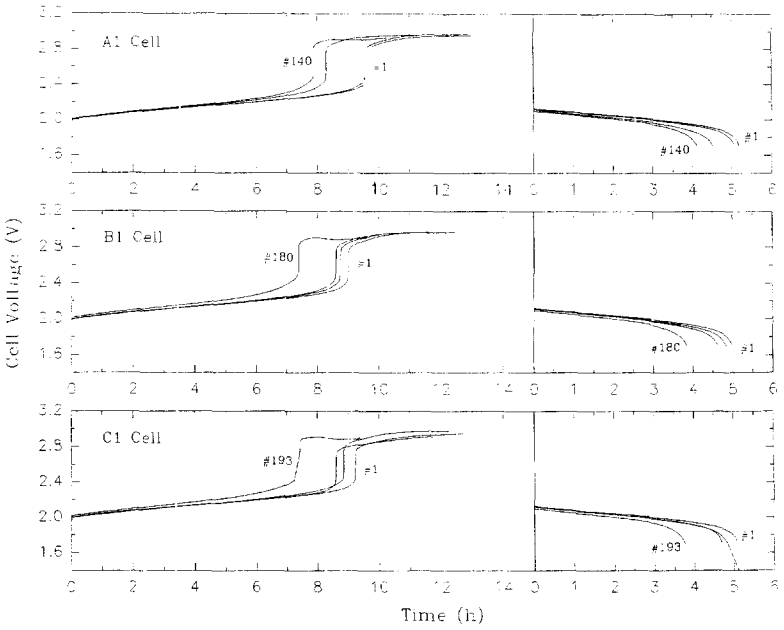

Fig. 4. Cell voltage at different cycles for cells A1, B1 and C1. Potential vs. time curves are identified for the first cycle and the last cycles, and the curves for intermediate cycles (#50, #100) are shown but not identified.

of the rate of capacity loss and the average delivered capacity per cycle, both based on the cell performance before the capacity dropped to 80% of the initial value. The rate of capacity loss rate, expressed as percentage per cycle, is based on the initial capacity and is estimated by

$$Y = \left(1 - C_{+}^{1/n}\right) \times 100 \quad (1)$$

where n denotes the total cycle number, C_+ represents the final fractional capacity (based on the initial cell capacity), and Y is the average capacity loss for each cycle. According to Table 2, group A has a higher initial capacity but a shorter cycle life, thereby causing a higher capacity loss per cycle. In contrast, group C has the lower capacity loss per cycle. The difference between the initial capacity and the capacity loss per cycle can be attributed to the phase composition of the positive plate. At a high curing temperature (85 °C), the predominant species are 4BS which favours the formation of α-PbO_2.

A higher α-PbO_2 content not only enhances the mechanical strength of the active-material but also exerts a beneficial effect on cycle life under deep-discharge service. Positive plates with high levels of β-PbO_2 display greater initial capacity since the surface area of β-PbO_2 exceeds that of α-PbO_2. In general, 3BS-rich material offers capacity while 4BS-rich material provides cycling capability [10]. Plots of capacity versus cycle number are given in Fig. 3 for cells A1, B1 and C1. The capacity of all cells reached their maximum values ($\sim$ 105–115%) after roughly 15 cycles, remaining above 80% up to 140 cycles at 100% depth-of-discharge (DOD). Increasing the curing temperature of positive plates gives rise to a lower initial capacity and a longer cycle life. Cell C1 exhibited a lower initial capacity but a longer cycle life. Fig. 4 depicts the cell voltage at various cycles for cells A1, B1 and C1. As the data reveal, all cells exhibit the expected shapes of charge and discharge curves.

Table 3
Cycle-life performance data for representative groups of 4.0 Ah VRLA cells under the ES-driving pattern

Sample	Cycle no.	Initial capacity (Ah)	Capacity loss/cycle (%)	Average capacity/cycle (Ah)
45 °C curing: Group A				
A6	64	3.41	0.348	3.18
A7	68	3.38	0.328	3.16
65 °C curing: Group B				
B6	76	3.15	0.293	3.02
B7	73	3.19	0.305	3.05
85 °C curing: Group C				
C6	87	3.08	0.256	3.04
C7	90	3.10	0.248	3.06

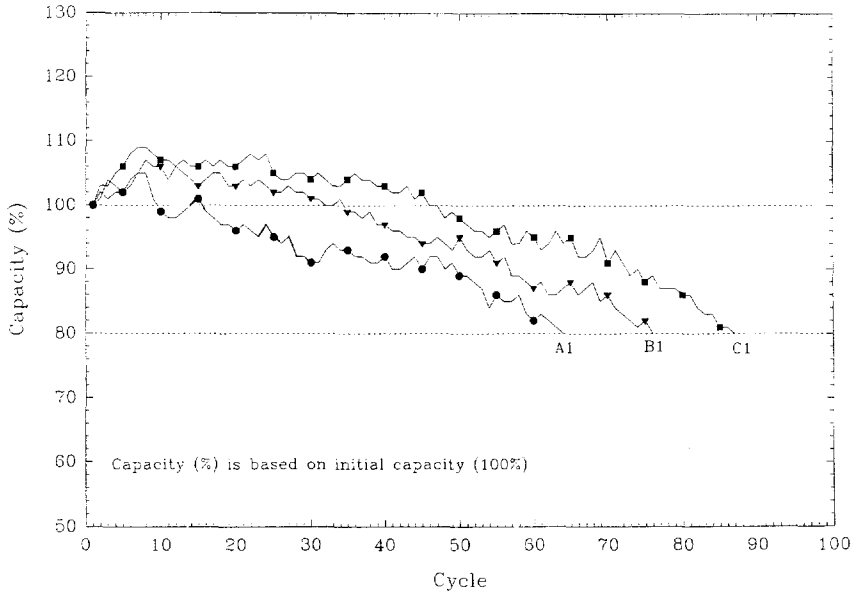

Fig. 5. Capacity vs. cycle number for cells A6, B6 and C6 under ES driving pattern given in Fig. 1(b).

3.3. Cell ES-driving pattern cycle-life performance

Two cells in each group were subjected to ES-driving pattern cycle testing to assess the influence of the three different curing temperatures listed in Table 3. Table 3 confirms that cells with plates cured at a low temperature have a higher initial capacity but shorter life and, thus, yield a higher capacity loss per cycle. Similar results can be found in Table 2. Capacity versus cycle number for cells A6, B6 and C6 under the ES-driving pattern are presented in Fig. 5. Similar to Fig. 3, the capacities of all cells reach their maximum values (~ 105–115%) after about 10 cycles, and remain above 80% for up to 70 cycles. Increasing the curing temperature of positive plates yields a lower initial capacity and a longer cycle life. Fig. 6 depicts the cell voltage and discharge current versus time during the first cycle for cells A6, B6, and C6. During the peak load (60 W kg^{-1}) period, the discharge current reaches the highest value while the cell voltage falls to its lowest level. Moreover, with each successive sub-cycle, the average voltage follows a downward trend and the discharge current increases. All of the cells complete about 30 sub-cycles before the terminal voltage falls to the cut-off value. The useful capacity per cell is calculated to be around 11 Ah/kg^{-1} and the equivalent range is about 21 km.

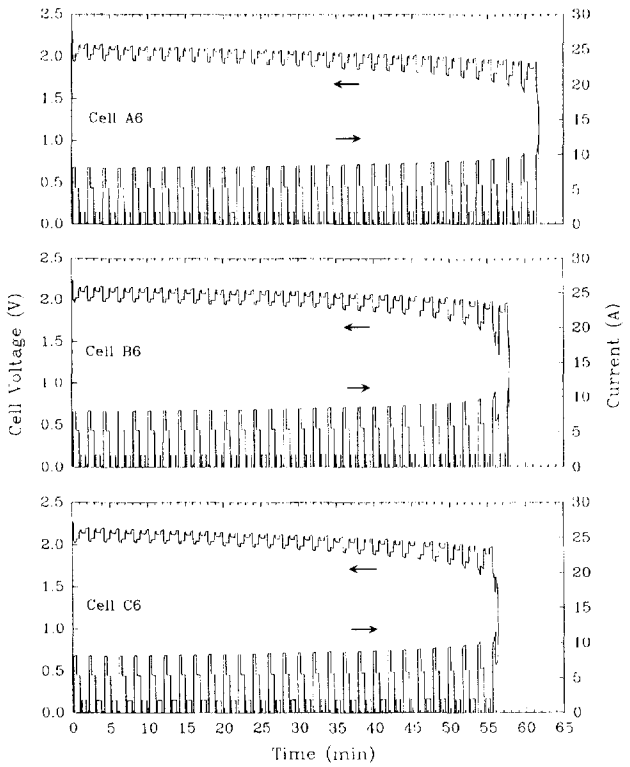

Fig. 6. Cell voltage and discharge current vs. time during the first cycle for cells A6, B6 and C6 under the ES-driving pattern given in Fig. 1(b).

4. Conclusions

Based on the results presented above, the following conclusions can be made.

1. Curing conditions obviously enhance the physico-chemical properties of the active-material of the positive plates as well as the electrochemical performance. The plates cured at higher temperature have less initial capacity but a longer cycle life for both testing methods (i.e., standard cycle testing and ES-driving pattern cycle testing).

2. During the formation, 4BS crystals undergo a meta-somatic conversion and produce PbO_2 crystals. This meta-somatic conversion produces PbO_2 while maintaining the

original morphology of the 4BS, and results in long life and cycleable lead/acid positive plates.

3. Results obtained from ES-driving cycle testing indicate that the useful capacity of VRLA cells is about 11 Ah kg^{-1} and the range is around 21 km.

4. A high curing temperature for the positive-plate materials enhances the cycle life under deep-discharge applications. Therefore, future research should concentrate on how to increase the utilization of positive plates at higher curing temperatures.

Acknowledgements

The author is grateful to the ROC National Science Council for financially supporting this work under Contract No. NSC-84-2214-E-214-003. Thanks are also due to the Ztong Yee Battery Corporation, Taiwan, for providing several electrodes and cell, parts.

References

[1] C.S. Syu and J.S. Chen, *Energy J.*, *24* (1994) 111–126 (in Chinese).
[2] D.A.J. Rand, R.J. Hill and M. McDonagh, *J. Power Sources*, *31* (1990) 203–215.
[3] J. Armstrong, I. Dugdale and W.J. McCusker, in D.H. Collins (ed.), *Power Sources 1966*, Pergamon, Oxford, 1967, pp. 163– 176.
[4] V. Iliev and D. Pavlov, *J. Appl. Electrochem.*, *9* (1979) 555–562.
[5] L. Zerroual, N. Chelali and F. Tedjar, *J. Power Sources*, *51* (1994) 425–431.
[6] J. Burbank, *J. Electrochem. Soc.*, *113* (1966) 10.
[7] G. Sterr, *Electrochim. Acta*, *15* (1970) 1221.
[8] B. Culpin, *J. Power Sources*, *25* (1989) 305–311.
[9] J.K. Vilhunen, S. Hornytzkyj and J. Tummavuori, *J. Power Sources*, *39* (1992) 59–65.
[10] D.A.J. Rand and L.T. Lam, *The Battery Man*, (Nov.) (1992) 18–28.